This article has been accepted for publication in a future issue of this journal, but has not been fully edited. Content may change prior to final publication. Citation information: DOI 10.1109/JLT.2018.2877305, Journal of Lightwave Technology

Robust Channel Estimation for Coherent Optical Orthogonal Chirp-Division Multiplexing with Pulse Compression and Noise Rejection

Xing Ouyang, *IEEE Member*, Cleitus Antony, Giuseppe Talli, and Paul Townsend

***Abstract*—Orthogonal chirp-division multiplexing (OCDM) was recently proposed as a promising modulation technique for high-speed fiber-optic communications due to its resilience to transmission impairments. By exploiting the pulse-compression property of the chirped waveforms, in this paper we propose a channel estimation algorithm compatible with the coherent optical (CO) OCDM system. In the proposed algorithm, a chirp from the orthogonal basis of the Fresnel transform is employed as the pilot signal. At the receiver, noise-rejection windowing is adopted in the Fresnel domain to remove the excessive noise after pulse compression, and then dispersions can be effectively compensated by efficient single-tap equalizers. It is shown that the proposed estimator is unbiased as long as the width of the noise-rejection window is wider than the maximum excess delay of the system. Moreover, the optimal window function achieving the minimum mean square error is derived in closed form. With these desired properties, it is shown that the proposed estimator outperforms conventional estimators, such as the intra-symbol frequency-domain average estimator, especially when the dispersion is severe. Finally, numerical results are provided to confirm the advantages of the CO-OCDM system with the proposed channel estimation algorithm.**

***Index Terms*—Optical coherent detection, chirp, pulse compression, orthogonal chirp-division multiplexing (OCDM), orthogonal frequency-division multiplexing (OFDM), channel estimation, intra-symbol frequency-domain average (ISFA), Fresnel transform.**

I. Introduction

FUELED by advances in optical and electronic technologies over the last two decades, optical communications has evolved into the advanced *Digital Era* to support the ever-increasing demand for high-speed data services [1-4]. With the advent of versatile digital signal processing (DSP) technology and coherent detection, advanced modulation formats and detection techniques have been demonstrated which realize the spectrally efficient transmission of high-capacity signals as well as flexible impairment compensation and improved receiver sensitivity [5-8]. For the next generation of lightwave systems, DSP will no doubt be a necessity for detecting high spectral efficiency (SE) signals in the presence of severe interference and distortion. For example, orthogonal frequency-division multiplexing (OFDM) is an advanced modulation technique that modulates a bank of narrowband subcarriers for delivering information. In this way, OFDM avoids inter-symbol interference (ISI) during transmission and compensates the subcarriers using efficient single-tap frequency domain equalizers [9-11].

Recently, a coherent optical (CO) orthogonal chirp-division multiplexing (OCDM) has been proposed as an advanced modulation technique for high-speed communications [12-14]. In CO-OCDM, symbols are modulated onto a set of orthogonal linear-frequency modulated waveforms (or chirps). The orthogonal chirps attain the Nyquist signaling rate at a maximum SE, and moreover contribute to the advantages of the OCDM signal. As a result OCDM exhibits better resilience against the impairments than, for example, the OFDM signals. In the CO-OCDM, the signals can be digitally synthesized by the discrete Fresnel transform (DFnT), which is realized efficiently by fast computation algorithms with digital circuits [15]. Moreover, due to the close relation of the Fourier and the Fresnel transforms, the CO-OCDM can be easily integrated into or adapted from traditional CO-OFDM systems with only minor changes, which makes the OCDM scheme is potentially easily deployable [13, 16, 17].

In the initial CO-OCDM proposal [13], channel estimation and equalization were realized by employing the conventional schemes designed for either OFDM systems in the frequency domain [18-21] or the single-carrier systems in the time domain [22-25]. Considering the similarity between OCDM and OFDM and the efficiency of the frequency-domain equalization (FDE), the frequency-domain schemes are more preferable. The existing algorithms designed for CO-OFDM can be readily adapted for OCDM. For example, the so-called intra-symbol frequency-domain averaging (ISFA) estimator, which is widely adopted in CO-OFDM systems to improve estimation accuracy [26-29], can be employed for the OCDM. Although the ISFA estimator can effectively suppress noise, it is however a biased estimator. As a result, its performance is considerably limited, especially when the dispersion is severe.

In this paper, we propose a channel estimator that is capable of utilizing the advantages of the chirped signals and is readily compatible with CO-OCDM. In the proposed algorithm, the pilot is a chirped signal directly obtained from the DFnT matrix. At the receiver, channel state information (CSI) is acquired by

This work was supported in part by the Science Foundation Ireland (SFI) (grant 12/IA/1270 and 12/RC/2276).

Xing Ouyang, Cleitus Antony, Giuseppe Talli, and Paul Townsend are with the Photonic System Group, Tyndall National Institute, Lee Maltings, Dyke Parade, Cork, T12 R5CP, Ireland (email: xing.ouyang@tyndall.ie; cleitus.antony@tyndall.ie; giuseppe.talli@tyndall.ie; paul.townsend@tyndall.ie).

This article has been accepted for publication in a future issue of this journal, but has not been fully edited. Content may change prior to final publication. Citation information: DOI 10.1109/JLT.2018.2877305, Journal of Lightwave Technology

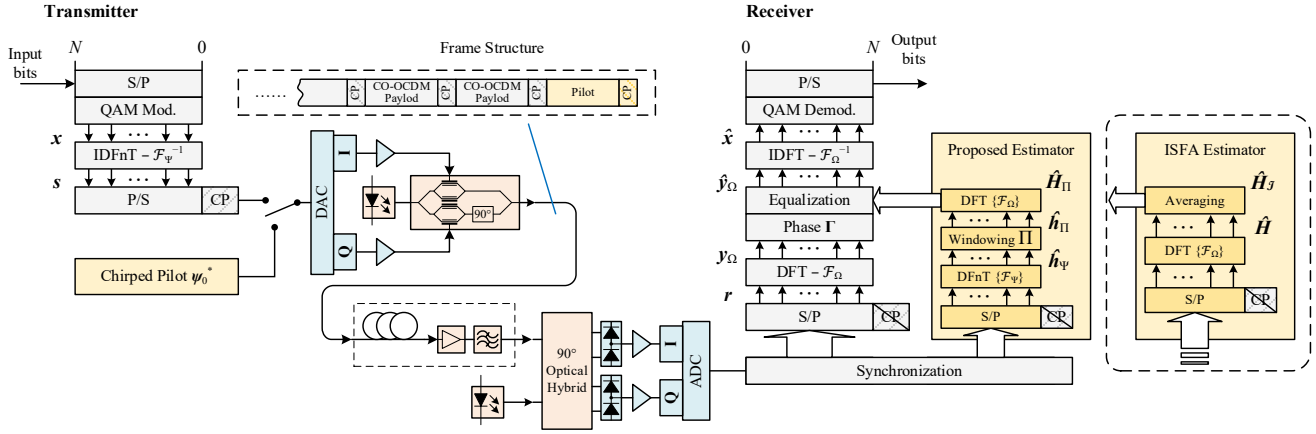

Fig. 1. System diagram of the CO-OCDM system with the proposed channel estimation algorithm.

exploiting the pulse-compression property of the chirped signal. That is, the impulse response function of the system is obtained by the pulse compression of the chirp. To improve the accuracy of the estimated CSI, a noise-rejection window is placed in the Fresnel domain to remove excessive noise. It is shown that the proposed estimator is unbiased and converges to the actual CSI of a system. Moreover, the optimal window function that attains the minimum mean square error (MSE) is derived in closed form. With these advantages, it will be shown in this paper that the proposed estimator outperforms other schemes, such as, the ISFA estimator, whilst it offers relatively low complexity with only one additional DFnT operation compared to the ISFA.

The paper is organized as follows. Section II introduces the CO-OCDM system model, and the proposed channel estimation algorithm is presented in Section III. In Section IV, the performance of the proposed estimator is analytically studied, and the optimal noise-rejection window achieving the minimum MSE (MMSE) is derived. In addition, practical implementation of the proposed estimator is discussed. In Section V, numerical results are provided to investigate the proposed estimator and also to validate the analysis in Section IV. Finally, conclusions are provided in Section VI.

Notations and Abbreviations: We use $\mathcal{F}_\Omega$ and $\mathcal{F}_\Omega^{-1}$ to denote the DFT and IDFT operators, respectively, and $\mathcal{F}_\Psi$ and $\mathcal{F}_\Psi^{-1}$ are the DFT and IDFT operators, respectively. The superscription $(\cdot)^*$ is complex conjugate, and $\otimes$ is the circular convolution operator. $\mathbf{E}\{\cdot\}$ denotes the expectation operator. Normally, we use a subscript $(\cdot)_\Omega$ to indicate signals in the Fourier (frequency) domain, and $(\cdot)_\Psi$ in the Fresnel domain. There are abbreviations specified in this paper; for example, channel impulse response (CIR), channel frequency response (CFR), channel state information (CSI).

II. System Model of CO-OCDM Systems

Fig. 1 illustrates the system diagram of a CO-OCDM system, in which information is modulated onto the orthogonal chirps, rather than the orthogonal subcarriers in CO-OFDM. Given that there are N chirps, the time-domain signal is generated by an inverse DFnT (IDFnT),

$$\begin{aligned} s(n) &= \mathcal{F}_\Psi^{-1}\{x(k)\}(n) \\ &= \sum_{k=0}^{N-1} x(k)\psi_k^*(n) \\ &= e^{j\frac{\pi}{4}} \sum_{k=0}^{N-1} x(k) \times \begin{cases} e^{-j\frac{\pi}{N}(k-n)^2} & \bmod N \equiv 0 \\ e^{-j\frac{\pi}{N}\left(k-n+\frac{1}{2}\right)^2} & \bmod N \equiv 1 \end{cases}, \end{aligned} \tag{1}$$

where $\mathcal{F}_\Psi$ is the DFnT operator and $\mathcal{F}_\Psi^{-1}$ the IDFnT operator, $x(k)$ is the symbol modulating the k-th chirp $\psi_k^*(n)$ and the superscript $(\cdot)^*$ is the complex conjugate operator. Considering the circular convolution-preservation property of the DFnT, a cyclic prefix (CP) is inserted between OCDM blocks to avoid inter-symbol interference (ISI) due to dispersion, bandwidth limitations and other impairments in the system [13]. The electrical signal is then amplified to drive an optical modulator for transmission. For simplicity, it is assumed that the modulator is operated within its linear region.

After fiber transmission, the signal is detected by a coherent receiver and converted to the electrical domain. At the receiver, if the channel impulse response (CIR) of the system is $h(n)$ and the additive white Gaussian noise (AWGN) is $v(n)$, the received signal after synchronization is

$$r(n) = h(n) \otimes s(n) + v(n), \tag{2}$$

where $\otimes$ denotes the circular convolution operator. Comparing Eqs. (1) and (2), one can intuitively apply the inverse operation, namely DFnT on $r(n)$, and the output of the DFnT is

$$\begin{aligned} y_\Psi(m) &= \mathcal{F}_\Psi\{h(n) \otimes s(n)\}(m) + \mathcal{F}_\Psi\{v(n)\} \\ &= h(m) \otimes x(m) + v_\Psi(m). \end{aligned} \tag{3}$$

In the above equation, the convolution-preservation property of the Fresnel transform is used to obtain the second equality [15]. It can be seen that the received signal, $y_\Psi(m)$, in the Fresnel domain is exactly the transmitted symbols, $x(m)$, circularly convolved with the CIR function, $h(m)$. In addition, it should be noted that the noise term in the Fresnel domain, $v_\Psi(m)$, is still AWGN of the same power as the DFnT is a unitary transform.

Inspecting Eq. (3), both time-domain equalization (TDE) and

This article has been accepted for publication in a future issue of this journal, but has not been fully edited. Content may change prior to final publication. Citation information: DOI 10.1109/JLT.2018.2877305, Journal of Lightwave Technology

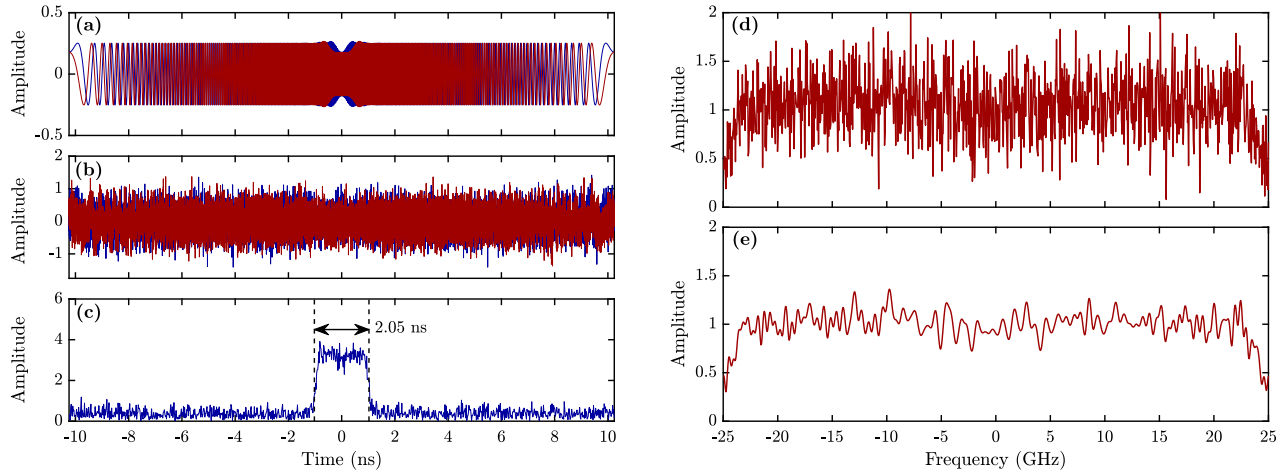

Fig. 2. One-shot observations of a 50 GHz CO-OCDM pilot signal after 320-km single-mode fiber transmission with a total dispersion ΔT_{CD} = 2.05 ns at an OSNR = 10 dB. Left: (a) transmitted time-domain pilot signal, (b) received pilot signal, and (c) the received signal after pulse compression. Right: (d) The corresponding amplitude of the estimated CFR without noise-rejection windowing and (e) that of the estimated CFR with noise-rejection windowing.

FDE can be adopted to compensate the dispersion $h(m)$. For example, if the FDE is adopted, a discrete Fourier transform (DFT) transforms the signal into the frequency domain for a single-tap FDE. An inverse DFT (IDFT) then converts the equalized signal back to the time domain for decision.

Alternatively, a simplified receiver scheme is adopted in this paper. As shown in Fig. 1, a DFT is performed on Eq. (2), rather than a DFnT. Based on the convolution theorem of DFT, one has

$$\begin{aligned} y_\Omega(m) &= \mathcal{F}_\Omega\{r(n)\}(m) \\ &= \mathcal{F}_\Omega\{h(n)\}(m)\times\mathcal{F}_\Omega\{s(n)\}(m)+\mathcal{F}_\Omega\{v(n)\}(m) \\ &= H(m)\times\mathcal{F}_\Omega\left\{\mathcal{F}_\Psi^{-1}\{x(k)\}\right\}(m)+v_\Omega(m). \end{aligned} \tag{4}$$

where $\mathcal{F}_\Omega$ is the DFT operator, H(m) is the channel frequency response (CFR), and $v_\Omega(m)$ is the noise in the frequency domain. Utilizing the eigen-decomposition of DFnT [15] gives

$$\mathcal{F}_\Omega\left\{\mathcal{F}_\Psi^{-1}\{x(k)\}\right\}(m)=\Gamma^*(m)\times\mathcal{F}_\Omega\{x(k)\}(m), \tag{5}$$

where $\Gamma(m)$ are the eigenvalues of DFnT with respect to DFT. Substituting it into Eq. (4), we then arrive at

$$y_\Omega(m)=H(m)\Gamma^*(m)\times\mathcal{F}_\Omega\{x(k)\}(m)+v_\Omega(m). \tag{6}$$

Once the CFR function, $H(m)$, is estimated by some means, the transmitted symbol can be recovered by single-tap equalization and phase rotations, following by another IDFT, as

$$\begin{aligned} \hat{x}(k) &= \mathcal{F}_\Omega^{-1}\left\{\left[H(m)\Gamma^*(m)\right]^{-1}\times y_\Omega(m)\right\}(k) \\ &= x(k)+\mathcal{F}_\Omega^{-1}\left\{\left[H(m)\Gamma^*(m)\right]^{-1}\times v_\Omega(m)\right\}(k). \end{aligned} \tag{7}$$

In Eqs. (4)-(7), except for the single-tap equalization, the receiver needs only two DFTs. Thus, the receiver in Fig. 1 is more computationally efficient than the conventional FDE scheme in Eq. (3) for the CO-OCDM, by saving one DFnT.

III. Proposed Channel Estimation Algorithm

In the proposed channel estimation algorithm, one orthogonal chirp is chosen from the Fresnel transform as the pilot signal for CSI acquisition, by utilizing the pulse-compression property of the chirped signal. Considering the finite-impulse-response (FIR) nature of practical communication systems, a windowing operation is applied after pulse compression to improve the estimation accuracy by removing the excessive noise. In the next section, the performance of the estimator is analytically studied, and the optimal window function achieving the MMSE is also derived in closed form.

A. Chirped Pilot for Pulse Compression

In the proposed channel estimation algorithm, the pilot signal is a chirp from the Fresnel transform, which is a column vector of the IDFnT matrix, i.e. $\psi_k^*(n)$ in Eq. (1). For example, if the k-th chirp is adopted at the pilot, one has the following relation

$$\mathcal{F}_\Psi\left\{\psi_k^*(n)\right\}=\delta(n-k), \tag{8}$$

where $\delta(k)$ is the Kronecker delta function. The received pilot can be obtained by substituting $s(n)$ in Eq. (2) with $\psi_k^*(n)$, as

$$r(n)=h(n)\otimes\psi_k^*(n)+v(n), \tag{9}$$

and after DFnT (pulse compression), it becomes

$$\begin{aligned} \hat{h}_\Psi(m) &= \mathcal{F}_\Psi\left\{r(n)\right\}(m)=h(m)\otimes\mathcal{F}_\Psi\left\{\psi_k^*(n)\right\}(m)+v_\Psi(m) \\ &= h(m-k)+v_\Psi(m). \end{aligned} \tag{10}$$

Thus, one can easily obtain the original CIR function, $h(m)$, by cyclically shifting $\hat{h}_\Psi(m)$ back by k steps. Without loss of generality, we say $\psi_0(n)$, for k = 0, is chosen as the pilot signal, as shown in Fig. 2 (a). The received pilot in the Fresnel domain in Eq. (10) is exactly the CIR function of the system corrupted by the additive noise, as illustrated in Fig. 2 (c). In a practical implementation, we need only one column of the IDFnT matrix,

This article has been accepted for publication in a future issue of this journal, but has not been fully edited. Content may change prior to final publication. Citation information: DOI 10.1109/JLT.2018.2877305, Journal of Lightwave Technology

say $\psi_0^*(n)$, for storage. The others can be generated by the circular-shift operation as the DFnT matrix is circulant.

At the receiver, if TDE is adopted, $\hat{h}_\Psi(m)$ can be readily used as the training sequence. FDE is considered in this paper since it is more computationally efficient in severely dispersive systems and more suitable for the CO-OCDM. The corresponding CFR function can be obtained by performing a DFT on Eq. (10), as

$$\begin{aligned}\hat{H}(m) &= \mathcal{F}_\Omega\left\{\hat{h}_\Psi(m)\right\} = \mathcal{F}_\Omega\left\{h(m)+v_\Psi(m)\right\} \\ &= H(m)+v_\Omega(m).\end{aligned} \tag{11}$$

Inspecting the system model as described in Eq. (10), the CIR function characterizes the effects resulting in pulse broadening, such as, the bandwidth-limitation effects of the electronic components of the transceiver, and the chromatic dispersion and the polarization-mode dispersion (PMD) in the fibers. In practical communication systems, the CIR function is time-limited, acting as an FIR filter. In other words, the CIR function, $h(n)$, is a linear filter with a finite number of non-zero taps. Given that the maximum excess delay of the system is ΔT_h, and synchronized and centered at $t = 0$, one has

$$h(n) = \begin{cases} h(n) & |n| \le \left\lceil \dfrac{\Delta L_h}{2} \right\rceil \\ 0 & \text{otherwise} \end{cases}, \tag{12}$$

where

$$\Delta L_h = \frac{\Delta T_h}{T_s} \tag{13}$$

is the normalized maximum excess delay of $h(n)$, with T_s being the sampling interval.

In Fig. 2 (c), the CIR function is illustrated considering a 50-GHz signal transmitted over a 320-km standard single-mode fiber (S-SMF) with a dispersion parameter of $D = 16$ ps/(nm·km) at 1550 nm. It is obtained by a DFnT on (b) the received chirped pilot with a received OSNR of 10 dB. It can be seen that the length of the pilot is about 20.5 ns. The pulse broadening due to chromatic dispersion is approximately 2.05 ns, showing the FIR feature of the fiber-optic system.

B. Noise-Rejection Windowing

If the estimated CFR function is directly obtained in Eq. (11), all the noise will be imposed on the CFR function, resulting in a noisy estimation, as shown in Fig. 2 (d). Considering the FIR feature of $h(n)$, it makes sense that the accuracy of the estimated CFR can be improved if we keep the significant CIR taps while removing unnecessary noise, on which the $h(n)$ are zero. For simplicity, if a gate function $\Pi_G(m)$ with a width of L_Π is chosen as the window function as an example, where

$$\Pi(m) = \Pi_G(m) = \begin{cases} 1 & |m| \le \dfrac{L_\Pi}{2} \\ 0 & \text{otherwise} \end{cases}, \tag{14}$$

the CFR function with noise-rejection windowing is thus

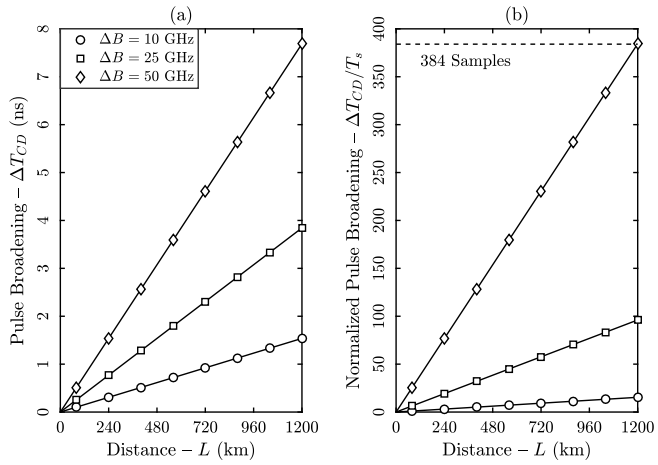

Fig. 3. (a) Pulse broadening and (b) normalized pulse broadening with respect to signal bandwidth versus fiber length by assuming a group velocity delay of $\beta_2 = 2.04 \times 10^{-26}$ s^2/m.

$$\begin{aligned}\hat{H}_\Pi(m) &= \mathcal{F}_\Omega\left\{\Pi_G(m)\times\hat{h}_\Psi(m)\right\} \\ &= \mathcal{F}_\Omega\left\{\Pi_G(m)\times h(m)\right\}+v_\Pi(m),\end{aligned} \tag{15}$$

where $v_\Pi(m)$ is the frequency-domain noise after windowing. In Fig. 2 (e), it can be observed that with a noise-rejection window, the estimated CFR function is much less noisy than that without the window in Fig. 2 (d).

In principle, the window should be no less than the maximum delay spread of the system. For a fiber-optic system, the delay spread comes from various sources. Taking chromatic dispersion, the principal dispersive effect in coherent systems, for example, the pulse broadening due to CD is

$$\Delta T_{\mathrm{CD}} = 2\pi\beta_2 L \times \Delta B \tag{16}$$

where ΔB is the signal bandwidth, and L and β_2 are the length and the group velocity dispersion (GVD) parameter of the fiber, respectively. In Fig. 3 (a), the pulse broadening due to CD, ΔT_{CD} is plotted as a function of the fiber length, whilst the normalized pulse broadening with respect to the signal bandwidth is shown in Fig. 3 (b). It can be seen that the pulse broadening due to CD varies quadratically with the system bandwidth. For a 25-GHz system, for example at 1200 km, the normalized pulse broadening is 96 samples, while for a 50-GHz system it increases to 384 samples. It will be shown later that this effect degrades the ISFA estimator significantly if the dispersion is severe or the signal bandwidth is relatively large.

In addition to CD, PMD in the fiber also contributes a small amount of pulse broadening. For example, the PMD in standard SMF is around 1 ps at 560 km, which in turn corresponds to merely 1 sample for a 50 GHz signal. There are also other linear effects introducing dispersions, such as the electronic components and filters in the transceiver, and optical filters in the fiber link. The ensemble pulse broadening can be approximated as

$$\Delta T_h \approx \Delta T_{\mathrm{CD}} + \Delta T_{\mathrm{PMD}} + \Delta T_{\mathrm{TX}} + \Delta T_{\mathrm{RX}} + \cdots, \tag{17}$$

This article has been accepted for publication in a future issue of this journal, but has not been fully edited. Content may change prior to final publication. Citation information: DOI 10.1109/JLT.2018.2877305, Journal of Lightwave Technology

where ΔT_{PMD}, ΔT_{TX}, and ΔT_{RX} denote the pulse broadening due to PMD, transmitter and receiver, respectively.

With the condition $L_\Pi > \Delta L_h$, we have the following relation

$$\hat{h}_\Pi(m) = \Pi_G(m)\hat{h}_\Psi(m) = h(m) + \Pi_G(m) \times v_\Psi(m), \tag{18}$$

and substituting it back into Eq. (15), we have

$$\hat{H}_\Pi(m) = H(m) + v_\Pi(m), \tag{19}$$

which is exactly the CFR corrupted by noise which is much less noisy. It can be easily seen from Eqs. (18) and (19) that if window width is larger than the maximum delay spread, the estimator $\hat{h}_\Pi$(m) or $\hat{H}_\Pi$(m) is unbiased to the actual CSI, namely, to the CIR, $h(n)$, in the time domain or to the CFR, $H(m)$, in the frequency domain.

In Fig. 1, the block diagrams of the proposed estimator and ISFA estimator are shown. It can be seen that the ISFA estimator needs one DFT and averaging operation [26]. Its complexity is in the order of $\mathcal{O}(0.5\times\log_2 N)$. The proposed estimator has one DFnT and one DFT, and the windowing operation. The DFnT can be calculated by using a fast algorithm that has similar complexity to that of the fast Fourier transform (FFT) with two additional phase rotation operations [12]. Thus, the proposed estimator needs only one more DFnT compared to the ISFA estimator, and it has a reasonably low complexity in the order of $\mathcal{O}(\log_2 N)$.

IV. Analysis and Discussions

In this section, the performance of the proposed estimator is analyzed in terms of the MSE. We will show that the proposed estimator asymptotically converges to the CSI under estimate. The optimum window function achieving the minimum MSE is also analytically derived. In addition, issues relating to the practical implementation are also discussed.

A. Mean Squared Error Performance

The MSE of the proposed estimator can be calculated as

$$\begin{aligned}\sigma_{\hat{H}}^2 &= \mathbf{E}\left\{\frac{1}{N}\sum_{m=0}^{N-1}\left|\hat{H}_\Pi(m) - H(m)\right|^2\right\} \\ &= \sigma_{\hat{h}}^2 = \mathbf{E}\left\{\frac{1}{N}\sum_{m=0}^{N-1}\left|\hat{h}_\Pi(m) - h(m)\right|^2\right\} \\ &= \frac{1}{N}\sum_{m=0}^{N-1}\left|\Pi(m)-1\right|^2\left|h(m)\right|^2 + \frac{\sigma_n^2}{N}\sum_{m=0}^{N-1}\left|\Pi(m)\right|^2\end{aligned} \tag{20}$$

where $\sigma_{\hat{h}}{}^2$ and $\sigma_{\hat{H}}{}^2$ are the MSE of $\hat{h}$ and $\hat{H}$, respectively, and $\sigma_n{}^2$ is the noise power. If the window function is the gate function in Eq. (14), the MSE can be further simplified, as

$$\sigma_{\hat{H}}^2 = \sigma_{\hat{h}}^2 = \begin{cases}\displaystyle\sum_{m=L_\Pi+1}^{\Delta L_h}\left|h(m)\right|^2 + \frac{L_\Pi}{N}\sigma_n^2 & L_\Pi < \Delta L_h \\ \displaystyle\frac{L_\Pi}{N}\sigma_n^2 & L_\Pi \geq \Delta L_h\end{cases}, \tag{21}$$

with a parameter L_Π, the width of the window function. Eq. (21) confirms that as long as the width of the noise-rejection window is wider than the maximum excess delay $L_\Pi > \Delta L_h$, the estimator is unbiased and asymmetrically converges to the actual CSI as the ratio (L_Π / N) becomes smaller.

B. MMSE Windowing Function

Though unbiasedness is a preferable attribute of an estimator, it is not necessarily a desired property when evaluating the performance of an estimator with respect to some practical criterion or loss function, for example, the MSE function. In other words, the unbiased estimator may not be optimal in terms of the minimum MSE, which is usually a desired property for an estimator to achieve.

To obtain the MMSE window function, we first differentiate the MSE function of $h(n)$ in Eq. (20) with respect to $\Pi(n)$, as

$$\frac{\partial\sigma_{\hat{h}}^2}{\partial\Pi(m)} = \frac{1}{N}\left[\Pi(m)-1\right]^*\left|h(m)\right|^2 + \frac{1}{N}\sigma_n^2\Pi^*(m). \tag{22}$$

Applying the MMSE condition that

$$\frac{\partial\sigma_{\hat{h}}^2}{\partial\Pi(m)} = 0, \tag{23}$$

and solving $\Pi(m)$, we have

$$\Pi_{\mathrm{MMSE}}(m) = \frac{\left|h(m)\right|^2}{\left|h(m)\right|^2 + \sigma_n^2}. \tag{24}$$

The MMSE window function in Eq. (24) can be regarded as a function of $h(n)$ when considering noise suppression. If $|h(m)|^2 \gg \sigma_n{}^2$, the weight is approximately 1, while it approaches zero in the region where $|h(m)|^2 \ll \sigma_n{}^2$. The MMSE of the proposed estimator can be accordingly calculated as

$$\min\sigma_{\hat{h}}^2 = \min\sigma_{\hat{H}}^2 = \frac{1}{N}\sum_{m=0}^{N-1}\frac{\left|h(m)\right|^2\sigma_n^2}{\left|h(m)\right|^2 + \sigma_n^2}. \tag{25}$$

C. Discussions on Practical Implementations

As discussed above, the proposed estimator can be either unbiased in Eq. (21) or optimally regarding the MMSE in Eq. (25). From a practical perspective, an unbiased estimator can be easily realized with a gate function once the receiver has the prior information of the maximum excess delay, which is determined by various effects, such as, dispersions and bandwidth-limited components. Considering that a fiber-optic system is time-limited, the window width, L_Π, can be chosen always slightly larger than the maximum delay which can be determined during system design by considering the effects indicated in Eq. (17). For example, in long-haul fiber systems, chromatic dispersion is the major dispersion source, which can be estimated by Eq. (16). The electronic components in the transceiver will also introduce pulse broadening. Nevertheless, as long as the signal is within the bandwidth of the components, they usually introduce only a small amount of pulse broadening. Thus, once the link is fixed, we can determine the window width by adding a small amount of redundancy to the estimated delay spread of the system. In the next section, we will show by numeric method that a certain amount of redundancy in the window width only introduces

This article has been accepted for publication in a future issue of this journal, but has not been fully edited. Content may change prior to final publication. Citation information: DOI 10.1109/JLT.2018.2877305, Journal of Lightwave Technology

negligible degradation.

In addition, in a well-designed OCDM system, the length of the guard interval is larger than the pulse broadening of the system. It can be inferred that in the worst case, if the width of the noise-rejection window is equal to the length of guard interval, then this ensures that the estimator is unbiased.

On the other hand, although the MMSE estimator is optimal in terms of MSE criterion, it requires a knowledge of the power profiles of the CIR, $|h(m)|^2$ and noise power, σ_n^2. As these quantities might not be known in practice, this issue requires more detailed consideration. Fortunately, gradient descent methods, such as, the least mean-square algorithm, can be adapted to find the MMSE solution. This paper will not consider this point further as it can be extended to the topic of adaptive estimation and equalization. Nevertheless, the MMSE performance in Eq. (25) can serve as a benchmark for the proposed estimator.

We investigate an example by choosing a Gaussian pulse,

$$h_{\text{in}}(t) = e^{-\pi \frac{t^2}{T_s^2}}, \tag{26}$$

transmitted through a standard SMF, where $T_s = 20$ ps (50 GHz) is the pulse width. The pulse at the output of the fiber is

$$h_{\text{out}}(t) = \frac{T_s}{\sqrt{T_s^2 - j \cdot 2\pi\beta_2 L}} e^{-\pi \frac{t^2}{T_s^2 - j \cdot 2\pi\beta_2 L}}, \tag{27}$$

where $\beta_2 = 2.04 \times 10^{-26}$ (s^2/m) is the GVD parameter of the fiber and L is the fiber length. The MMSE window function can be obtained in closed form by substituting Eq. (27) into (24), and the MMSE can be calculated by using Eq. (25).

If the gate function is adopted, Eq. (21) can be used to numerically to evaluate the MSE. The MSE of a gate function is plotted in Fig. 4, as a function of the received OSNR and normalized window size η_Π, which is defined as

$$\eta_\Pi = \frac{L_\Pi}{\Delta L_{\text{CD}}}. \tag{28}$$

where $\Delta L_{\text{CD}} = \Delta T_{\text{CD}} / T_s$ is the normalized pulse broadening of CD. It can be seen that the optimal η_Π for a gate function varies depending on the OSNR and is about 2 to 3 times of the broadening due to CD. This is because the Gaussian function is not well temporally-confined and has a large tail spreading over the time axis.

It should be noted that, rather than the Gaussian function, the pulse shaping filter in practical systems is usually a square function (zero-order interpolation), a raised cosine function, or other Nyquist pulses, which can be well shaped in time. Thus, it can be inferred that the optimum width for the gate window will be smaller, which will be shown in the following section by numeric simulations.

V. Simulations and Performance Evaluations

In this section, simulations were carried out to study the performance of the CO-OCDM system with the proposed channel estimator (CO-OCDM/Prop.). In addition, the ISFA estimator was implemented in the simulation for both the traditional CO-OFDM and CO-OCDM systems to provide a direct comparison.

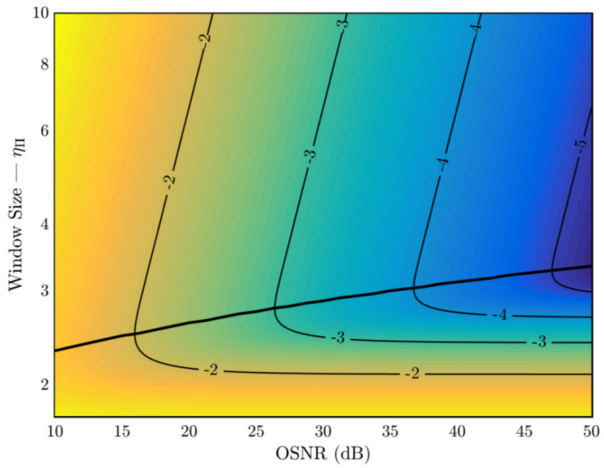

Fig. 4. The analytical mean square error of the proposed estimator by considering a Gaussian pulse transmitting through 320-km SMF, by assuming that the SMF has a group velocity dispersion (GVD) parameter of $\beta_2 = 2.04 \times 10^{-26}$.

The system setup is shown in Fig. 1. At the transmitter, the sampling rate of the DACs is 50 GSa/s. In the simulation, up-sampling is performed by using a raised-cosine filter with a roll-off factor of 0.05 and up-sampling factor of 4. In addition, the raised cosine can emulate the bandwidth limitation effect in the system. The laser is operated at 1550 nm and the optical modulator is assumed to be operated within linear region. In the system, standard SMF (S-SMF) is considered with an attenuation of 0.2 dB/km and a dispersion parameter of 16 ps/(nm·km) at 1550 nm. In this paper, to focus on the performance of the proposed estimator with respect to the analysis in Section IV, we only consider chromatic dispersion in the fiber, which is the dominant dispersive effect in the SMF. This allows us to systematically compare the numerical results with the analytical results in the previous section.

In the CO-OFDM, there are 1024 subcarriers, of which 892 subcarriers are modulated with payload. The remaining subcarriers are nulls for the purpose of oversampling. The OFDM signal thus has a bandwidth of 43.75 GHz. In the CO-OCDM, there are 892 orthogonal chirps. With an oversampling rate of 8 / 7, the number of samples of an OCDM symbol block is also 1024 with a bandwidth of 43.75 GHz for a fair comparison. For both systems, the length of the GI is 384 samples to accommodate a dispersion of up to 7.68 ns, corresponding to a fiber length of 1200 km, as indicated in Fig. 3 (b). It should be noted that the pulse-shaping filter and resampling process at the receiver will also introduce additional bandwidth limitations on the signals.

A. MSE Performance

In Fig. 5, the MSE of the proposed estimator is investigated at (a) 240 km, (b) 480 km and (c) 640 km, by adjusting the normalized window width. Similar results to those in Fig. 4 can be observed. It should be noted that as the length of fiber increases, the normalized optimal window width, η_Π, gets slightly smaller. The reason is that, apart from the chromatic dispersion, there are other effects causing a certain amount of pulse broadening, e.g., the pulse shaping filter and resampling filter. For example,

This article has been accepted for publication in a future issue of this journal, but has not been fully edited. Content may change prior to final publication. Citation information: DOI 10.1109/JLT.2018.2877305, Journal of Lightwave Technology

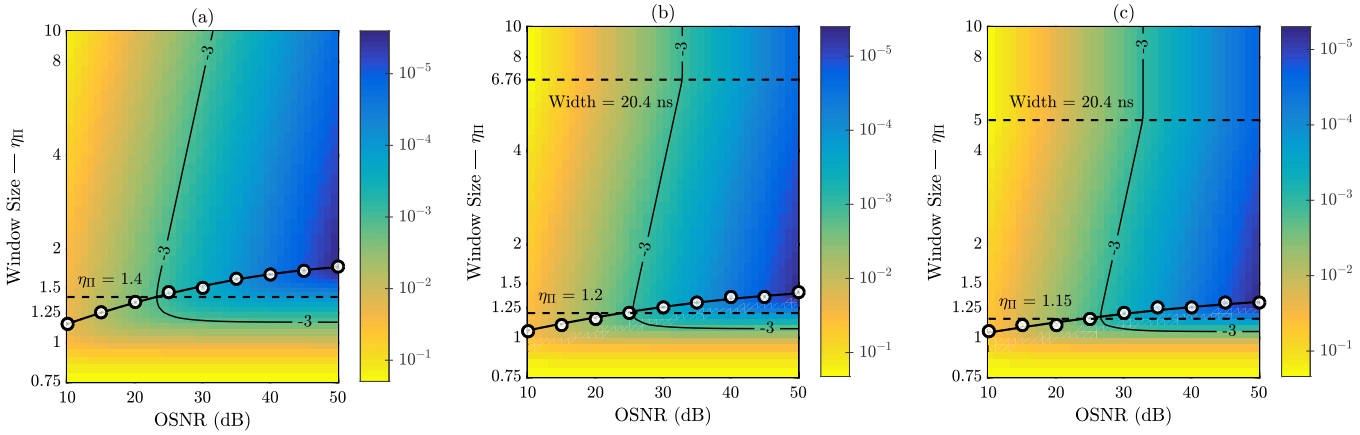

Fig. 5. Simulated mean square errors of the proposed channel estimator as a function the received OSNR and the normalized window size η_Π after (a) 240-km, (b) 480-km, and (c) 640-km transmission; the contour lines denote MSE $\sigma_h^2 = \sigma_H^2 = 1\times10^{-3}$; the lines with hollow circles indicate the trace of the lowest MSE. It can be seen that the optimal normalized windows sizes η_Π are (a) 1.4, (b) 1.2, and (c) 1.15 to achieve a MSE of 1×10^{-3} with a minimal OSNR.

to achieve a MSE = 10^{-3}, the optimal window sizes are η_Π = (a) 1.4, (b) 1.2, and (c) 1.15, respectively. Referring to Appendix A, the extra pulse broadening excluding the contribution from chromatic dispersion can be calculated as about 0.62 ns, which accounts for the shift of the optimal normalized window size. The overall pulse broadening of the system is approximated by $\Delta T_{\mathrm{CD}} + \tau_\Pi$. In addition, for the cases of (b) 480 km and (c) 640 km, it can be seen that the improvement starts to saturate as the window width becomes larger than 20 ns, which is the length of the pilot signal.

In Fig. 6, the MSE performance between the proposed and ISFA estimators are compared. The dotted lines represent the optimal MSE (hollow circles) in Fig. 5. More importantly, the performance of the proposed estimator shows only slight degradation compared to the optimal lines in the low OSNR region, and converges to the optimal lines in the high OSNR region by choosing a fixed window width that is sufficient to accommodate the pulse spreading.

The MSE of the ISFA estimator with different numbers of averaging taps is also shown. In the case of 240 km, for example, the performance of the ISFA estimator improves as the number of averaging taps, $\|\mathcal{D}\|$, goes up from 3 to 9, for OSNR < 15 dB, where the noise dominates the performance degradation. So increasing the number of averaging taps can efficiently suppress the noise. As the OSNR increases, the performance of ISFA with larger $\|\mathcal{D}\|$ starts to degrade. The reason is that the bias of the ISFA estimator results in a deviation from the actual CSI of the system, and larger the $\|\mathcal{D}\|$ is, the more divergence becomes. In the high OSNR region, the deviation begins to dominate the degradation as the noise becomes smaller. For OSNR > 30 dB, the ISFA estimator with 3 taps performs the best. In contrast, the proposed estimator always attains better performance than the ISFA, especially for longer fiber transmission distance. It can be seen that the ISFA estimator of $\|\mathcal{D}\| = 9$ does not work for a distance greater than 240 km. Even for the ISFA estimator of $\|\mathcal{D}\| = 3$, MSE floors occur at 9×10^{-4} and 3×10^{-3} at distances of 480 km and 640 km, respectively.

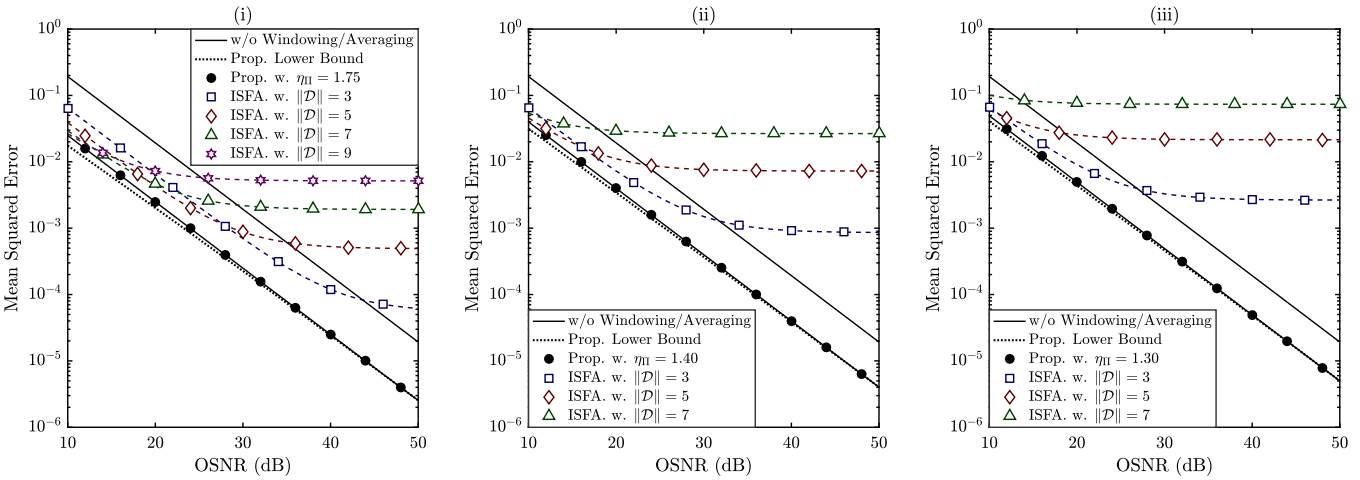

Fig. 6. Simulated mean square errors of the proposed channel estimator (solid circles) and that of the ISFA estimator (hollow markers) versus OSNR after (i) 240-km, (ii) 480-km , and (iii) 640-km transmission; the dotted lines are the lowest MSE with an optimal window size as indicated by the lines with hollow circles in Fig. 5. For the proposed estimator (the lines with solid circles), the windows size are chosen to be η_Π = (i) 1.75, (ii) 1.40, and (iii) 1.30 to achieve an optimal MSE at the OSNR of 50 dB. As a result, it can be observed that the lines with solid circles asymptotically converge to the dotted lines.

This article has been accepted for publication in a future issue of this journal, but has not been fully edited. Content may change prior to final publication. Citation information: DOI 10.1109/JLT.2018.2877305, Journal of Lightwave Technology

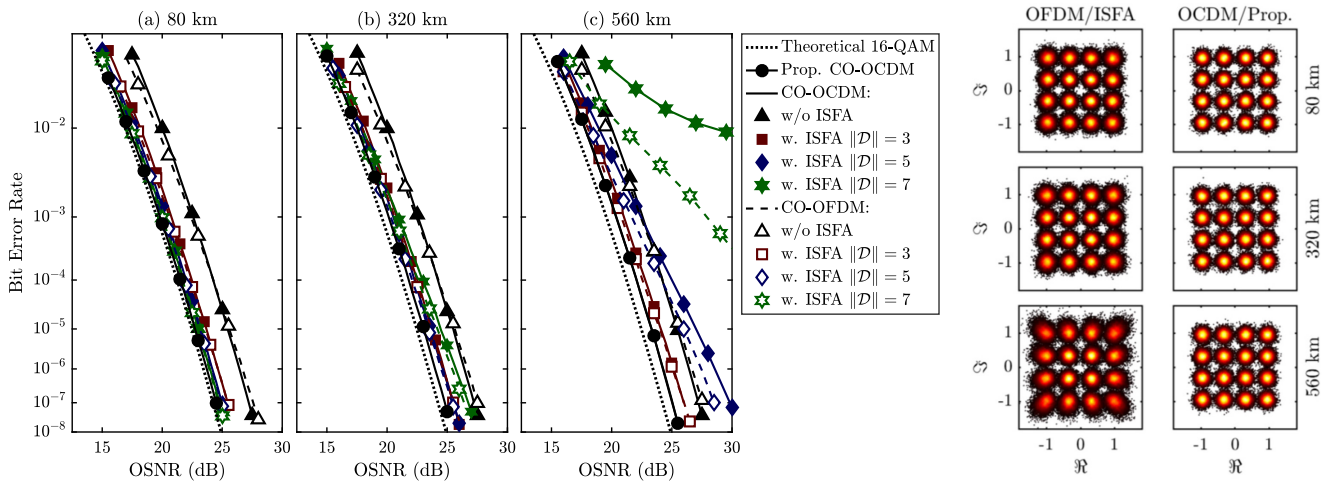

Fig. 7. Left: BER performance of the CO-OFDM systems with ISFA estimator and the CO-OCDM systems with the proposed channel estimator with 16-QAM at (a) 80 km, (b) 320 km and (c) 560 km. Right: the received constellation diagrams with a received OSNR = 20 dB.

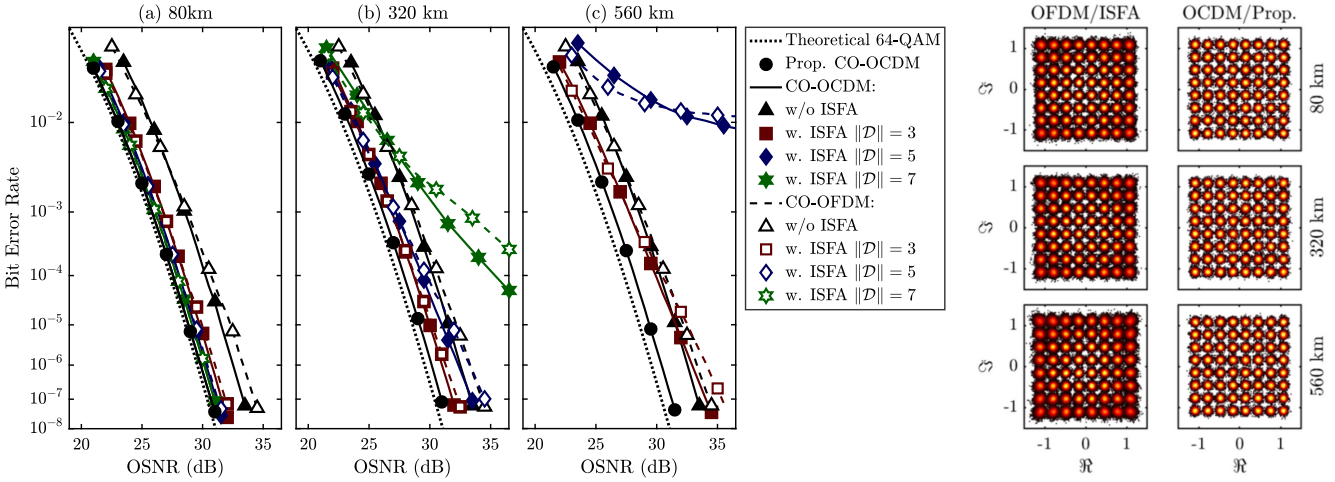

Fig. 8. Left: BER performance of the CO-OFDM systems with ISFA estimator and the CO-OCDM systems with the proposed channel estimator with 64-QAM at (a) 80 km, (b) 320 km and (c) 560 km. Right: the received constellation diagrams with a received OSNR = 26 dB.

B. Bit-Error Rate Performance

The bit-error rate (BER) performance of the proposed CO-OCDM is investigated in comparison with the ISFA estimator for both CO-OFDM and CO-OCDM systems with 16-QAM in Fig. 7 and 64-QAM in Fig. 8, respectively.

In the case of 16-QAM in Fig. 7, the performance is evaluated at (a) 80 km, (b) 320 km, and (c) 560 km, and the maximum number of averaging taps of the ISFA estimator is 7. At 80 km, the performance of the CO-OFDM/ISFA and CO-OCDM/ISFA improves as the number of averaging taps increases from 3 to 7. When the distance goes up to 320 km in Fig. 7 (b), the ISFA estimator with $\|\mathcal{D}\| = 7$ slightly degrades compared to the cases of $\|\mathcal{D}\| = 3$ and 5 in the high OSNR region > 20 dB. If the distance increases to 560 km, both systems with ISFA $\|\mathcal{D}\| = 7$ are significantly degraded. Even reducing the number of averaging taps to 5, it has worse performance than the OFDM and OCDM systems without ISFA for the OSNR > 25 dB. The trends match the analyses in Fig. 6 because the distortion in ISFA becomes unacceptable if $\|\mathcal{D}\|$ is large and/or the dispersion is relatively severe. The constellation diagrams of the received signals are shown on the right of Fig. 7 by fixing the averaging taps to $\|\mathcal{D}\| = 5$. It can be seen that the distortion expands the constellations outwards and causes decision errors.

In Fig. 7 (a) at 80 km, the theoretical performance of the 16-QAM signal is attained with the proposed estimator. As the distance increases to 320 km and 560 km, only slightly degradation occurs, as observed from the BER curves (solid circles) shifting to the right by less than ~1 dB in OSNR. The negligible degradation results from the estimation errors due to the increased pulse broadening along with the increase of chromatic dispersion, which can be interpreted using Eq. (21).

In Fig. 8, 64-QAM is adopted instead, and similar results can be observed. For the proposed CO-OCDM, the BER curves are shifted to the right by ~6 dB in OSNR compared to the results in Fig. 7 as the Euclidean distance of 64-QAM signal is smaller than that of 16-QAM signal. In Fig. 8 (a), for the ISFA estimator, there is no obvious degradation and the ISFA estimator with $\|\mathcal{D}\| = 7$ has better performance than $\|\mathcal{D}\| = 3$ and 5 because the dispersion in an 80-km SMF is negligible. However, significant degradation occurs as the distance goes up to and beyond 320

This article has been accepted for publication in a future issue of this journal, but has not been fully edited. Content may change prior to final publication. Citation information: DOI 10.1109/JLT.2018.2877305, Journal of Lightwave Technology

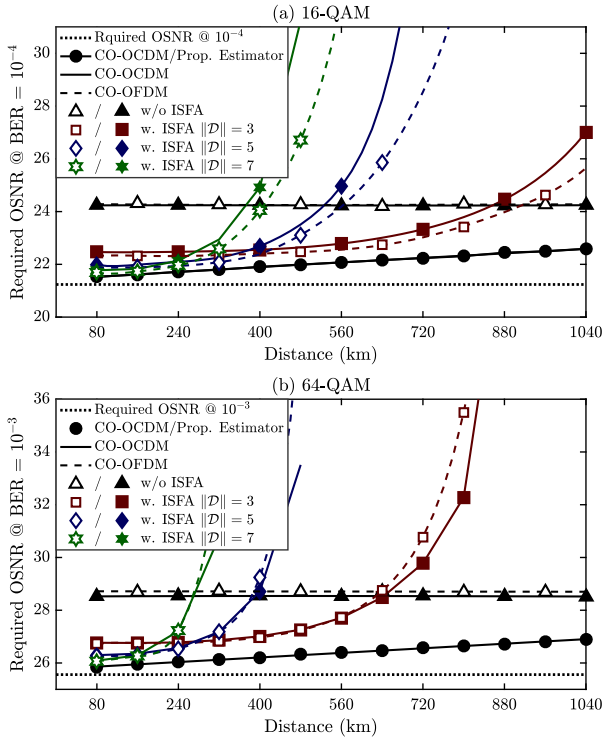

Fig. 9. The OSNR penalty of single polarization systems based on the proposed CO-OCDM and the CO-OFDM/ISFA with (a) 16-QAM and (b) 64-QAM.

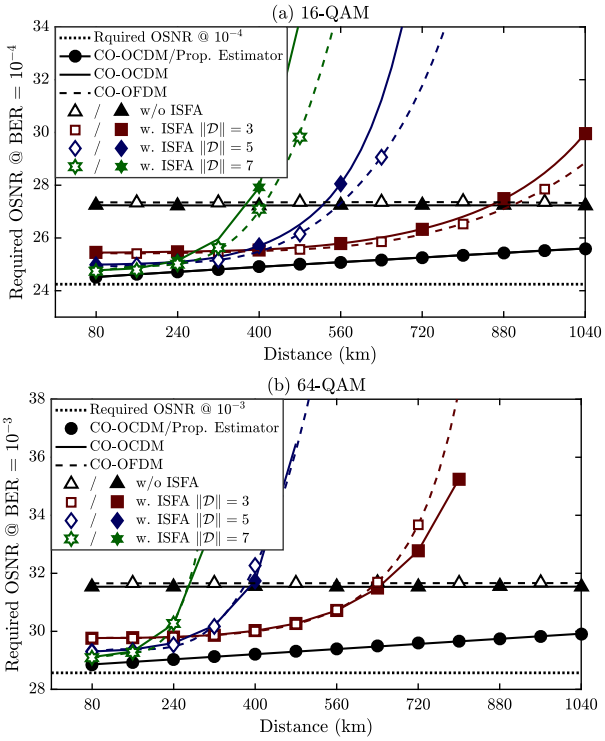

Fig. 10. The OSNR penalty of PDM systems based on the proposed CO-OCDM and the CO-OFDM/ISFA with (a) 16-QAM and (b) 64-QAM.

km. For example, at a distance of 320 km, obvious degradation occurs in Fig. 8 (b) as the OSNR is larger than 26 dB for 5 and 7 taps. If the distance increases to 560 km, the CO-OFDM/ISFA with 7 averaging taps no longer works. Even for $\|\mathcal{D}\| = 5$, a BER floor is observed at BER = 1×10^{-2}.

The degradation of the ISFA estimator for 64-QAM in Fig. 8 arises because high-level modulation formats are more sensitive to noise and distortion. Comparing the ISFA estimator in Fig. 7 and 8, in the case of 16-QAM, CO-OFDM achieves better performance, while for 64-QAM CO-OCDM does better. The reason is that the CO-OCDM is more prone to the deviation error of ISFA and thus it has worse performance than the CO-OFDM as shown in Fig. 7. As the modulation level goes to 64-QAM in Fig. 8, the CO-OCDM system achieves better performance because high-level modulation formats are more sensitive to distortions while CO-OCDM is more robust to the distortions than CO-OFDM.

In both Fig. 7 and 8, the proposed CO-OCDM scheme always achieves the best performance, approaching the theoretical limits for both 16-QAM and 64-QAM signals because the proposed estimator introduces no bias to the CO-OCDM system.

C. *Transmission Performance*

In Fig. 9, the required OSNR to achieve a fixed BER level is plotted against transmission distance for 16-QAM at 1×10^{-4} and 64-QAM at 1×10^{-3}, respectively. It can be seen that both cases without noise averaging show almost no performance degradation as the estimation error does not change with distance. Instead, it only depends on the OSNR level. The ISFA estimator exhibits similar behavior for both formats. In the short distance region, the ISFA estimator with a larger number of averaging taps has better performance. If the distance increases, the ISFA estimator with more averaging taps starts to degrade first and it requires higher OSNR than the system without noise averaging at a given distance.

For both modulation levels, the proposed CO-OCDM has superior performance compared to the other examples. The OSNR penalty increases slightly by about 1 dB as the distance increases from 80 to 1040 km. The minor increase in the required OSNR is due to the increase of chromatic dispersion, as indicated in Eq. (21).

To further study the proposed estimator, a polarization-division multiplexing (PDM) system is adopted. To adapt the proposed estimator for the PDM system, the correlated dual-polarization (CDP) based pilot structure is adopted for the proposed chirped pilot to estimate the polarization state of the system [30]. More specifically, in the proposed estimator, there are two symbols slots for the chirped pilots, i.e., $[\psi_0^*, \psi_0^*]^T$ in the X-polarization and $[\psi_0^*, -\psi_0^*]^T$ in the Y-polarization. At the receiver, the Jones matrix of the dual-polarization system can be easily estimated based on the CDP algorithm in [30] for signal recovery. In addition, the CDP can also be easily applied for the ISFA estimator as well.

The results are shown in Fig. 10. The PDM systems achieve similar performance to the single-polarization systems in Fig. 9, but with doubled data rates. Comparing the results in Fig. 9 and Fig. 10, the PDM systems require 3-dB higher OSNR compared to the single-polarization systems which is to be expected since the signal power is measured as the sum of the two polarizations. Beside this difference, there is no discernible penalty for the PDM system, which confirms that the CO-OCDM system with the proposed estimator can work in a dual polarization scheme

and that it also has the best performance amongst the schemes compared in this paper.

VI. Conclusion

In this paper, a channel estimation algorithm is proposed specifically for CO-OCDM, which utilizes the pulse-compression property of the chirped CO-OCDM signal. At the receiver, considering the FIR-feature of the system, the performance of the proposed estimator can be improved by removing the excessive noise with a noise-rejection window. In the paper, the optimum MMSE window is also derived as the bench mark for the proposed estimator. Detailed analyses are provided to investigate the proposed CO-OCDM system, and numerical results are also provided to validate its advantages in comparison with the ISFA estimator. It is shown that the proposed estimator can be readily compatible with the CO-OCDM systems of single-polarization and PDM and improve the performance significantly. As a result, the proposed estimator is a practical and attractive channel estimator for the CO-OCDM. Moreover, as the OCDM is an advanced modulation technique that is resilient to system impairments, the proposed estimator further makes it an attractive candidate to realize high-speed fiber-optic communications.

Appendix A

The extra window width Δ_Π, by excluding the pulse broadening due to chromatic dispersion, needed to optimally achieve a MSE = 10^{-3} can be calculated using the following equation

$$\begin{aligned}\tau_\Pi &= L_\Pi \times T_s - \Delta T_{CD} \\ &= \eta_\Pi \Delta L_{CD} \times T_s - \Delta T_{CD} = \eta_\Pi \Delta T_{CD} - \Delta T_{CD} \\ &= (\eta_\Pi - 1)\Delta T_{CD}.\end{aligned} \tag{29}$$

By substituting Eq. (16) into (29), and using the parameters that $\beta 2 = 2.04 \times 10^{-26}$, η_Π = (a) 1.4, (b) 1.2, and (c) 1.15, L = (a) 240, (b) 480, and (c) 640 km, the extra width can be calculated as τ_Π = (a) 0.6152, (b) 0.6152, and (c) 0.6153 ns. Therefore, the pulse broadening excluding the contribution from chromatic dispersion is about 0.62 ns.

References

[1] G. Li, "Recent advances in coherent optical communication," *Advances in Optics and Photonics,* vol. 1, no. 2, pp. 279-307, Apr. 2009.

[2] H. Rohde *et al.*, "Coherent ultra dense WDM technology for next generation optical metro and access networks," *J. Lightw. Technol.,* vol. 32, no. 10, pp. 2041-2052, May 2014.

[3] A. Shahpari *et al.*, "Coherent access: a review," *J. Lightw. Technol.,* vol. 35, no. 4, pp. 1050-1058, Feb. 2017.

[4] P. J. Winzer and D. T. Neilson, "From scaling disparities to integrated parallelism: A decathlon for a decade," *J. Lightw. Technol.,* vol. 35, no. 5, pp. 1099-1115, Mar. 2017.

[5] P. J. Winzer and R. J. Essiambre, "Advanced optical modulation formats," *Proc. IEEE,* vol. 94, no. 5, pp. 952-985, May 2006.

[6] S. J. Savory, "Digital coherent optical receivers: algorithms and subsystems," *IEEE J. Sel. Top. Quantum Electron.,* vol. 16, no. 5, pp. 1164-1179, Sept. 2010.

[7] P. J. Winzer, "High-spectral-efficiency optical modulation formats," *J. Lightw. Technol.,* vol. 30, no. 24, pp. 3824-3835, Dec. 2012.

[8] S. Beppu *et al.*, "2048 QAM (66 Gbit/s) single-carrier coherent optical transmission over 150 km with a potential SE of 15.3 bit/s/Hz," *Opt. Express,* vol. 23, no. 4, pp. 4960-4969, Feb. 2015.

[9] W. Shieh and C. Athaudage, "Coherent optical orthogonal frequency division multiplexing," *Electron. Lett.,* vol. 42, no. 10, pp. 587-589, May 2006.

[10] J. Armstrong, "OFDM for optical communications," *J. Lightw. Technol.,* vol. 27, no. 1-4, pp. 189-204, Feb. 2009.

[11] R. Giddings, "Real-time digital signal processing for optical OFDM-based future optical access networks," *J. Lightw. Technol.,* vol. 32, no. 4, pp. 553-570, Feb. 2014.

[12] X. Ouyang and J. Zhao, "Orthogonal chirp division multiplexing," *IEEE Trans. Commun.,* vol. 64, no. 9, pp. 3946-3957, Jul. 2016.

[13] — —, "Orthogonal chirp division multiplexing for coherent optical fiber communications," *J. Lightw. Technol.,* vol. 34, no. 18, pp. 4376-4386, Aug. 2016.

[14] X. Ouyang *et al.*, "Chirp spread spectrum toward the Nyquist signaling rate — Orthogonality Condition and Applications," *IEEE Signal Process. Lett.,* vol. 24, no. 10, pp. 1488-1492, Aug. 2017.

[15] X. Ouyang *et al.*, "Discrete Fresnel transform and its circular convolution property," *arXiv.org,* vol. arXiv:1510.00574, 2015.

[16] X. Ouyang *et al.*, "Intensity-modulation direct-detection OCDM system based on digital up-conversion," in *Proc. CLEO*, San Jose, California, 2018, p. SM2C.2.

[17] X. Ouyang *et al.*, "Experimental demonstration of 112 Gbit/s orthogonal chirp-division multiplexing based on digital up-conversion for IM/DD systems with improved resilience to system impairments," in *Proc. 2018 ECOC*, Rome, Italy, 2017, p. Mo4F.

[18] Y. S. Liu *et al.*, "Channel estimation for OFDM," *IEEE Communications Surveys and Tutorials,* vol. 16, no. 4, pp. 1891-1908, 2014.

[19] H. Meng-Han and W. Che-Ho, "Channel estimation for OFDM systems based on comb-type pilot arrangement in frequency selective fading channels," *IEEE Trans. Consum. Electron.,* vol. 44, no. 1, pp. 217-225, 1998.

[20] L. Ye, "Pilot-symbol-aided channel estimation for OFDM in wireless systems," *IEEE Trans. Veh. Technol.,* vol. 49, no. 4, pp. 1207-1215, 2000.

[21] W. Shieh, "Maximum-likelihood phase and channel estimation for coherent optical OFDM," *IEEE Photon. Technol. Lett.,* vol. 20, no. 8, pp. 605-607, 2008.

[22] V. Lottici *et al.*, "Channel estimation for ultra-wideband communications," *IEEE J. Sel. Areas Commun.,* vol. 20, no. 9, pp. 1638-1645, 2002.

[23] D.-S. Ly-Gagnon *et al.*, "Coherent detection of optical quadrature phase-shift keying signals with carrier phase estimation," *J. Lightw. Technol.,* vol. 24, no. 1, p. 12, Jan. 2006.

[24] G. Colavolpe *et al.*, "Robust multilevel coherent optical systems with linear processing at the receiver," *J. Lightw. Technol.,* vol. 27, no. 13, pp. 2357-2369, Jul. 2009.

[25] D. Falconer *et al.*, "Frequency domain equalization for single-carrier broadband wireless systems," *IEEE Commun. Mag.,* vol. 40, no. 4, pp. 58-66, Apr. 2002.

[26] X. Liu and F. Buchali, "Intra-symbol frequency-domain averaging based channel estimation for coherent optical OFDM," *Opt. Express,* vol. 16, no. 26, pp. 21944-21957, Dec. 2008.

[27] X. Liu *et al.*, "448-Gb/s reduced-guard-interval CO-OFDM transmission over 2000 km of ultra-large-area fiber and five 80-GHz-grid ROADMs," *J. Lightw. Technol.,* vol. 29, no. 4, pp. 483-490, Feb. 2011.

[28] F. Li *et al.*, "High-level QAM OFDM system using DML for low-cost short reach optical communications," *IEEE Photon. Technol. Lett.,* vol. 26, no. 9, pp. 941-944, May 2014.

[29] Q. Chen *et al.*, "FFT-size efficient 4096-QAM OFDM for low-cost DML-based IMDD system," *IEEE Photon. J.,* vol. 8, no. 5, pp. 1-10, Oct. 2016.

[30] X. Liu *et al.*, "Improving the nonlinear tolerance of polarization-division-multiplexed CO-OFDM in long-haul fiber transmission," *J. Lightw. Technol.,* vol. 27, no. 16, pp. 3632-3640, Aug. 2009.

Xing Ouyang (M'09) received his M.Sc. degree in Information Science and Engineering from Dalian Polytechnic University, China in 2013, and a PhD in Electrical and Electronic Engineering from Tyndall National Institute, University College Cork, Ireland in 2017.

During his PhD, he was in the Photonic Systems Group, Tyndall National Institute, engaged in advanced digital signal processing technology for next-generation fiber-optic communication. In 2016, he was with Nanyang Technological University, Singapore, involved in the "Car-to-Car WiFi: Multi-Hop Video Streaming" project. He is now a researcher in the Photonic Systems Group, Tyndall National Institute, Cork, Ireland. His research topics include advanced DSP techniques, such as modulation formats, OFDM, and channel equalization, and their applications in both fiber-optic and radio-frequency systems.

Cleitus Antony (M'09) received B.E. and M.Sc. degrees in electrical engineering and physics, respectively, from Birla Institute of Technology and Science, Pilani, India, in 2001, and a Ph.D. in physics from the Photonics Systems Group, Tyndall National Institute and the Department of Physics, University College Cork, Cork, Ireland, in 2011.

From 2001 to 2006, he was with Opnext Japan, Inc., Yokohama, Japan, and was involved in the design and development of fiber-optic transceivers conforming to the 10 Gbit Ethernet standard. During his Ph.D. he was engaged in developing novel burst-mode transmission techniques at data rates of 10 Gbits/s in long-reach passive optical networks. He is currently a senior postdoctoral researcher in the Photonics Systems Group, Tyndall National Institute, where his research activities include next-generation optical access networks and fiber-optic distributed sensors. He holds five patents in the field of optical telecommunications and has authored more than 40 peer-reviewed publications.

Giuseppe Talli (S'01–M'03) received the Laurea degree in electronic engineering from the University of Padova, Padova, Italy, in 2000 and the Ph.D. degree in electronic engineering from the University of Essex, Essex, U.K., in 2003, for work on the effects of the amplified spontaneous emission in semiconductor optical amplifiers and their gain dynamics.

Since 2004, 2004 to 2008 he has been with the Photonic Systems Group at the Tyndall National Institute, University College Cork, Ireland, as a post-doctoral scientist. From 2008 to 2012 has been with Intune Networks, Dublin, working on design and implementation of photonic subsystems for optical burst switching in metro networks. Since July 2012 he has rejoined the Tyndall National Institute as staff research scientist, working in the area of next generation optical access networks including metro-scale passive optical network (PON) architectures and burst-mode subsystems.

Paul D. Townsend (M'04) received the B.Sc. degree in physics from the University of East Anglia, Norwich, U.K., in 1983 and the Ph.D. degree in physics from the University of Cambridge, Cambridge, U.K., in 1987.

From 1987 to 1990, he held a joint position with St. John's College, Cambridge, and with Bellcore, Red Bank, NJ, and in 1990, he joined British Telecom Laboratories, Ipswich, U.K., where he worked on various aspects of quantum optics and optical communications including quantum cryptography. In 2000, he joined the Corning Research Centre, Ipswich, where he was a Project Manager for access network applications research. Since 2003, he has been with the Tyndall National Institute and the Department of Physics, University College Cork, in Ireland, where he is a Research Professor. He is currently Head of Photonics at Tyndall and Director of the Irish Photonic Integration Centre (IPIC). His research interests include optical and quantum communications. Prof.. Townsend is a Fellow of the Institute of Physics (U.K. and Ireland)